Supplemental Information

Dual autogenous control of the multiple antibiotic resistance phenotype in *Escherichia coli*

Guillermo Rodrigo, Djordje Bajić, Ignacio Elola, and Juan F. Poyatos

Table of Contents

Supplementary Experimental Methods……………………………………………..…..2
Strains construction
Culture media and reagents
Quantification of fluorescence in a cell population
Analysis of fluorescence data
Quantification of mRNA levels by qRT-PCR
Quantification of fluorescence in single cells
Analysis of single cell images
Quantification of fluorescence by flow cytometry

Supplementary Mathematical Methods……………………………………………...9
Empirical model of the dynamic response
Bottom-up mathematical model
Note on the negative autogenous control of the system
Simplification of the mathematical model
Analytical solutions of the model I: temporal behavior
Analytical solutions of the model II: dynamic range
Signal transduction and de-repression
Apparent transfer function and stress cross-talk
Stochastic modeling
Note on the potential excitability of the system

Supplementary Figures and Figure Legends……………………………………..20

Supplementary Tables……………………………………………………………38

Supplementary References………………………………………………………40

Supplementary Experimental Methods

Strains construction

We engineered a two-color fluorescent reporter strain (*Escherichia coli*) to measure the activity of the *marRAB* promoter, following the work by Miyashiro & Goulian (2007)[1]. The strain (named as IE01) contains a chromosomal copy of the *yfp* gene (Yellow Fluorescent Protein) under the control of the *marRAB* promoter, and the *cfp* gene (Cyan Fluorescent Protein) expressed with a constitutive *tetA* promoter at the attachment sites in *E. coli* of lambda and HK022 phages, respectively.

To construct the YFP reporter, we amplified the promoter region of the *marRAB* operon (1616883-1617144) by PCR. The primers used were: 5’-TAGCAGAATTCCGGCAGCAAC (forward), and 5’-GCATAGGGATCCTGGCAAGTAAT (reverse). The PCR product was then cloned it into a plasmid (pTM74; Miyashiro & Goulian, 2007) that contains a multicloning site upstream of the promoterless *yfp* gene to yield the plasmid pJFP01 (this work). This plasmid was integrated as single copy into the lambda phage attachment site of *E. coli* MG1655 using the helper plasmid pInt-TS (Weiss *et al.*, 1999). The residual *cat* gene linked to the *marRAB* promoter was replaced by *kan* by electroporating a PCR product created from the template plasmid pKD4 into the appropriate strain carrying plasmid pKD46 to yield the strain JFP01 (this work). The two-color reporter strain JFP02 was created by moving the previous marker into strain TIM64 (a strain derived from a MG1655 that constitutively expresses CFP; TIM64 does not present any antibiotic resistance marker; Miyashiro & Goulian, 2007) by P1 transduction. Removal of the *kan* marker using plasmid pCP20 originated *E. coli* strain IE01. This was verified by PCR. In addition, *E. coli* strain IE02 was constructed by deletion of the *rob* gene in IE01 with the application of a Datsenko & Wanner (2000) knockout protocol followed by the removal of the *kan* marker using plasmid pCP20 (Datsenko & Wanner, 2000). The primers used were: 5’-ATATCCCAATGGCATCGTAAAGAACATTTTGAGGCATTTCAGTCAGTTGCGCTGGAGCTGCTTCGAA (forward), and 5’-ATGAACCTGAATCGCCAGCGGCATCAGCACCTTGTCGCCTTGCGTATAATATGAATATCCTCCTTAG (reverse). The sequence of the resulting strain was verified by PCR.

---

[1] We thank Tim Miyashiro for strains, and Mark Goulian for strains and experimental advice.

We also constructed a strain deleting the *marB* gene (named as DB01)[2]. This was done from strain IE01 using a variant of the Datsenko & Wanner (2000) knockout protocol, with the insert (*kan* marker with *marB* flanking regions) obtained by PCR from a KEIO collection strain (Baba *et al.*, 2006). Strain IE01 containing the pKD46 plasmid was electroporated with this insert in presence of arabinose, allowing recombination in the *marB* locus. The primers used to obtain the insert were: 5’-GACCAATATGCAGGGCGAATCG (forward), and 5’-ATGTATTTGGCTTGCGGTGG (reverse). Correct substitution of the *marB* gene by *kan* marker was checked by PCR and sequencing.

Culture media and reagents

Medium LB was always used for overnight cultures. Minimal medium M9 (M9 salts 1x, $MgSO_4$ 2 mM, $CaCl_2$ 0.1 mM, glucose 0.4%, casamino acids 0.05%, vitamine B1 0.05%) was used to grow cells during characterization experiments. To induce the *mar* circuit, we used different concentrations of Salicylate (Sigma), resulting in a gradient ranging from 0 to 5 mM, and also different concentrations of cAMP (Sigma), resulting in a gradient ranging from 0 to 20 mM. When appropriate, we used kanamycin at a concentration of 50 μg/mL.

---

[2] We thank Jerónimo Rodríguez-Beltrán for practical assistance.

Quantification of fluorescence in a cell population

Experiments of induction were carried out to study the dynamics of the system. Cultures (volume of 2 mL) inoculated from single colonies (three replicates) were grown overnight in LB medium supplemented with glucose 0.4% at temperature of 37 ºC and shaking of 170 rpm. Cultures were then diluted 1:200 in M9 minimal medium (10 μL of culture into a final volume of 2 mL) and were grown for 2 h at temperature of 37 ºC and shaking of 170 rpm. Cultures were then used to load the multiwell plate (Thermo) with final volumes of 200 μL. Per well, we added directly a volume of the culture, a volume of salicylate stock, and a volume of cAMP stock (when appropriate)[3].

The set up for the Victor X2 was as follows. OD_{600} measured with absorbance filter of 600 nm (0.5 s for reading). YFP measured with excitation filter of 497/16 nm, and emission filter of 535/40 nm. CFP measured with excitation filter of 434/17 nm, and emission filter of 479/40 nm. For both YFP and CFP, we took 8000 for energy lamp, and 0.1 s for counting. Temperature was at 37 ºC. The program started first with OD_{600}, then YFP, and finally CFP, followed by 30 s of shaking in orbital mode. Then it waited for 5 min, and it started again.

---

[3] We also used mineral oil for characterization. Cultures were grown as previously indicated, and then were used to load the multiwell plate (Thermo) with final volumes of 250 μL. Per well, we added directly 200 μL of culture (counting the volume of inducers), and 50 μL of mineral oil (Sigma). However, we found that the *mar* circuit does not respond to salicylate in anaerobic conditions.

Analysis of fluorescence data

We collected time-course data of fluorescence (YFP and CFP) and absorbance. Background values of absorbance and fluorescence, which corresponded to M9 minimal medium, were subtracted to correct the signals. The normalized fluorescence (for both YFP and CFP) was calculated as the ratio of fluorescence and absorbance. Similar values of normalized fluorescence were reported for MG1655 cells and for M9 minimal medium, which indicated that the auto-fluorescence of cells was negligible in this case. The growth rate of cells was calculated as the slope of the linear regression between the log of corrected absorbance and time in exponential phase. Time-dependent promoter activity, defined as the instantaneous production rate of normalized YFP fluorescence (magnitude per cell), was calculated for each time point using the derivative of the normalized fluorescence. Promoter activity in steady state, defined as the stationary production rate of normalized YFP fluorescence (magnitude per cell) in exponential phase, was calculated as the average over time (for $t > 2$ h) of normalized fluorescence times growth rate. The error associated to that measure was obtained by calculating the standard deviation over replicates in all time points, then squaring all these deviations to average them, and finally getting the root square. Data were analyzed with Matlab (MathWorks).

Quantification of mRNA levels by qRT-PCR

Cultures (volume of 2 mL) inoculated from single colonies (three replicates) were grown overnight in LB medium at temperature of 37 ºC and shaking of 170 rpm.

Cultures were then diluted 1:200 in M9 minimal medium (10 μL of culture into a final volume of 2 mL) and were grown for 2 h at temperature of 37 ºC and shaking of 170 rpm. Then, aliquots of 1.5 mL were quickly pelleted by centrifuging 2 min at 13,000 rpm and resuspended in 50 μL of TE buffer (10 mM Tris-HCl, pH 8.0, 1 mM EDTA). Bacteria were broken by adding 50 μL of a mix 1:1 phenol:chloroform (pH 8.0) and vortexing thoroughly. Bacterial RNA from each sample was recovered in the aqueous phase by centrifuging 5 min at 13,000 rpm. A subsequent re-extraction was done by adding 50 μL chloroform followed by centrifugation of 5 min at 13,000 rpm, recovering the aqueous phase. Samples were then passed through a silica-based, DNA-clean column (Zymo) and were eluted in 8 μL of TE buffer. DNase I (Fermentas) was added (1 U) for 1 h at 37 ºC, which was then thermally inactivated (30 min at 65 ºC) by adding EDTA. Total RNA eluted was quantified in a NanoDrop.

One-step SYBR PrimerScript RT-PCR Kit II (Takara) was used for detection, following the Kit protocol for preparing the reaction volumes. 16S rRNA was used as housekeeping gene to normalize RNA quantity in each reaction. The primers for qRT-PCR were synthesized by IDT for *marA* and Sigma for 16S rRNA. The primer sequences for amplifying *marA* were taken from (Viveiros *et al.*, 2007) and for 16S rRNA from (Carothers *et al.*, 2011). Reactions in triplicate were carried out using a Step One Plus Real-Time PCR System (Applied Biosystems). The thermal cycling program for amplification was 5 min at 42°C, 10 s at 95°C, and 40 cycles of 5 s at 95°C and 34 s at 60°C (Shuttle PCR); following with default melting curves[4].

---

[4] We thank Eszter Majer for help with the RNA extraction and Anouk Willemsen for help with the qRT-PCR.

Quantification of fluorescence in single cells

Experiments of induction were carried out to study the heterogeneity of the dynamic response. Culture (volume of 2 mL) inoculated from a single colony was grown overnight in LB medium supplemented with glucose 0.4% at temperature of 37 ºC and shaking of 170 rpm. Culture was then diluted 1:200 in M9 minimal medium (10 μL of culture into a final volume of 2 mL) and was grown for 4 h at temperature of 37 ºC and shaking of 170 rpm. The different cultures diluted 1:10 were then used to load the agarose pads.

Agarose pads were prepared with a volume of 5 mL of M9 minimal medium and 0.075 g of agarose. It was dissolved by vortexing and microwaving. The pads were then allowed to solidify for about 1 h at room temperature before seeding bacteria. 2 μL of each culture were then used to load the pads. They were kept for about 15 min at room temperature so that cells can be absorbed into the agarose. Just before characterization with the microscope, 2.5 μL salicylate from a solution 0.1 M was used to induce cells in solid medium, having estimated the volume of the agarose pad in 50 μL (resulting concentration of salicylate about 5 mM).

In each pad, fields with an adequate initial density of cells were chosen, the first photo was taken, and salicylate was added. Photos were taken for each field every 12 minutes.

Agarose pads were monitored in an inverted microscope Axiovert200 (Zeiss) with objective 100X/1.45 oil Plan-Fluar at temperature of 30 ºC. The microscope was equipped with a digital camera C9100-02 (Hamamatsu), a Xenon lamp XBO 75W/2, an optical filter changer Lambda 10-2 (Sutter), a motorized stage (Marzhauser), and a temperature controller (Cell Observer-Zeiss). Moreover, the microscope was automated by the commercial software MetaMorph (Universal Imaging). Cell images were acquired from the bright-field and fluorescence channels. We used the fluorescence filters yellow FP (490-510 nm, 510-560 nm) and cyan FP (426-446 nm, 460-500 nm).

Analysis of single cell images

Microscopy photos were segmented and analyzed using the EBImage package for R from Bioconductor. Segmentation allowed us to identify sets of pixels belonging to individual cells, and measure the average apparent YFP and CFP intensities for each of these sets. The ratio YFP/CFP was used as proxy for system activity.

Quantification of fluorescence by flow cytometry

Cultures (volume of 2 mL) inoculated from single colonies were grown overnight in LB medium without and with 5 mM salicylate at temperature of 37 ºC and shaking of 170 rpm (to have uninduced and pre-induced cultures). These cultures were subsequently diluted 1:200 in 2 mL of M9 minimal medium with different concentrations of salicylate (0, 0.05, 0.25, 0.5, 2.5 and 5 mM). After incubation for 4h at the same conditions, cells were spun down and resuspended in PBS buffer. YFP (525 nm) intensity was measured in the flow cytometer Gallios (Beckman-Coulter). YFP distributions were obtained with a standard flow cytometry analysis (software Kaluza).

Supplementary Mathematical Methods

Empirical model of the dynamic response

Our reporter protein (YFP) monitors the promoter activity of the *marRAB* operon (P_{mar}). Then, we can write

$$\frac{d}{dt}[YFP] = \Pi_{mar} - \mu[YFP] \qquad \text{(S1)}$$

where μ is the cell growth rate and Π_{mar} the activity of promoter P_{mar}. Empirically, we proposed the following exponential model

$$\frac{[YFP](t)}{[YFP]_{\infty}} = \left(1 - e^{-\lambda t}\right)^{m} \qquad \text{(S2)}$$

where λ and m are two parameters that control the dynamics of the response, and $[YFP]_{\infty}$ is the concentration in steady state. We fitted with our own experimental data by nonlinear regression the parameters λ and m. Combining Eqs. (S1) and (S2), promoter activity was calculated as

$$\Pi_{mar} = \left(\frac{m\lambda}{e^{\lambda t} - 1} + \mu\right)\left(1 - e^{-\lambda t}\right)^{m} . \qquad \text{(S3)}$$

The time to reach the 50% of the steady state value (t_{50}) upon induction with salicylate reads

$$t_{50} = \frac{-1}{\lambda}\ln\left(1 - \frac{1}{2^{1/m}}\right) . \qquad \text{(S4)}$$

We also considered the response speed, here defined as $\frac{1}{[YFP]}\frac{d[YFP]}{dt}$ and evaluated at t_{50}. This gives $\ln(2)\lambda$ for Eq. (S2) and $m >> 1$. In case of a non-regulated gene, whose dynamics is governed by $\left(1 - e^{-\mu t}\right)$, the response speed is directly μ. In addition, differentiating Eq. (S3), we calculated the time where promoter activity is maximal (τ), given by

$$\tau = \frac{1}{\lambda}\ln\left(\frac{m\lambda - \mu}{\lambda - \mu}\right). \qquad \text{(S5)}$$

We used this model to fit either population or single cell experimental data.

Bottom-up mathematical model

We constructed a system of ordinary differential equations (ODEs) by knowing the topology of the circuit. MarR, MarA and MarB form an operon controlled by promoter P_{mar} (Alekshun & Levy, 1997; Chubiz *et al*., 2012). MarR represses P_{mar}, which can be modulated by salicylate (Cohen *et al*., 1993). MarB also represses P_{mar} (Vinué *et al*., 2013), whereas MarA activates it (Martin *et al*., 1996). On the other hand, Rob is controlled by promoter P_{rob}, and it activates P_{mar} (Alekshun & Levy, 1997). MarA and Rob repress P_{rob} (Schneiders & Levy, 2006). Finally, in our system YFP models a downstream gene controlled by promoter P_{mar}. Although MarR, MarA and MarB are transcribed from the same promoter, the corresponding protein expressions may be different each other due to distinct translation rates. By analyzing the 5' untranslated regions of MarR, MarA and MarB with RBS calculator (Salis *et al*., 2009), considering the 30 nucleotides upstream and the 7 nucleotides downstream of the start codon, we found that translation rates of MarA and MarB are about 30-fold and 20-fold, respectively, higher than the translation rate of MarR. This is in tune with previous experimental observations (Martin & Rosner, 2004). In addition, promoter P_{mar} is regulated by CRP-cAMP. Therefore, we could write

$$
\begin{aligned}
&\frac{d}{dt}[MarA] = \beta\Pi_{mar} - (\mu+\delta)[MarA] \\
&\frac{d}{dt}[MarR] = \Pi_{mar} - \mu[MarR] \\
&\frac{d}{dt}[MarB] = \beta^{*}\Pi_{mar} - \mu[MarB] \qquad\qquad (S7) \\
&\frac{d}{dt}[Rob] = \Pi_{rob} - \mu[Rob] \\
&\frac{d}{dt}[YFP] = \Pi_{mar} - \mu[YFP],
\end{aligned}
$$

where μ is the cell growth rate, δ the degradation rate of MarA ($\delta >> \mu$), noting that MarA is quickly degraded by protease Lon (Griffith *et al.*, 2004), β (and β^{*}) the fold increase of MarA (MarB) translation rate, and Π_{mar} and Π_{rob} the activity of promoters P_{mar} and P_{rob}, respectively.

The equations for Π_{mar} and Π_{rob}, knowing that MarA and Rob act as monomers whereas MarR as a dimer (Martin *et al.*, 1996), could be approached by Hill functions (Bintu *et al.*, 2005). However, we knew that the effect of MarA on P_{rob} is not observable in physiological conditions (Chubiz *et al.*, 2012), so we neglected this regulation to simplify the system of equations. We also demonstrated in this work by qRT-PCR that MarB does not repress P_{mar} in presence of salicylate, whereas MarB indeed represses P_{mar} in absence of salicylate. This also led us to eliminate MarB from the model. Therefore, it turned out

$$
\Pi_{mar} = \Pi_0 \frac{1 + f_a[MarA]/K_A + f_b Q([Rob],[cAMP])}{1 + [MarA]/K_A + Q([Rob],[cAMP])} \frac{1}{1 + \left([MarR_{free}]/K_R\right)^2}, \qquad (S8)
$$

where K_A, and K_R are the effective dissociation constants for transcription regulation, and f_a and f_b the activation fold changes. Π_0 is the basal protein synthesis rate, and Q a regulatory function that accounts for the activation of Rob and CRP-cAMP. Phenomenologically, and assuming competitive binding between the three transcriptional activators (MarA, Rob and CRP-cAMP) as their operators overlap, we can write

$$Q([Rob],[cAMP]) = \left([Rob]/K_B\right) + \left([cAMP]/K_C\right), \qquad \text{(S9)}$$

where K_B and K_C are the effective dissociation constants for transcription regulation. This model can explain that, in presence of Rob or cAMP, MarA does not increase significantly the occupancy of polymerase at the *marRAB* promoter, which agrees with previous experimental and theoretical data (Wall *et al.*, 2009). In addition, we have

$$[MarR_{free}] = \frac{1 + \alpha\left([Sal]/\theta_S\right)^{\nu_S}}{1 + \left([Sal]/\theta_S\right)^{\nu_S}}[MarR], \qquad \text{(S10)}$$

where θ_S is the effective dissociation constant between salicylate (Sal) and MaR, ν_S the Hill coefficient, and α the minimal fraction of free MarR.

Note on the negative autogenous control of the system

In addition to MarR and MarA, the *marRAB* operon contains another open reading frame coding for a small periplasmic protein. Recently, MarB has been identified as a repressor of the *marRAB* promoter (Vinué *et al.*, 2013), establishing a new putative negative feedback into the system. To study this novel regulation on the dynamic response, we knocked out the *marB* gene. A quantification of transcripts revealed that MarB is not able to repress the expression of the *marRAB* operon in presence of salicylate, although MarB does repress the operon in absence of it (Fig. S2N), which is tune with previous results (Vinué *et al.*, 2013). We confirmed by fluorescence assays the observation that MarB does not repress the *marRAB* promoter upon induction with salicylate, even for moderate concentrations of this inducer (Fig. S2M). While MarB does not impact the dynamic range, we observed that the Δ*marB* system exhibits a slower response to salicylate. Our results suggested that the bacterial cell might exploit MarB as an enhancer of MarR to tightly repress the operon. They also revealed that Rob and MarB are regulatory elements that contribute to a fast mounting of the *mar* phenotype.

Simplification of the mathematical model

Our bottom-up mathematical model can be simplified for a better analysis of the dynamic response. By noting $x = [MarA]/K_R$, $y = [MarR]/K_R$, $y_0 = [MarR_{free}]/K_R$ (the concentration of MarR is equal to the one of YFP), $\rho = f_a = f_b$ (assuming for simplicity equal induction by the three transcriptional activators), $\pi_0 = \Pi_0/K_R$, and also $\kappa = K_R/K_A$, we could write a simplified system of ODEs. We also denoted by z ($[Rob]/K_B$) and c ($[cAMP]/K_C$) the normalized concentrations of Rob and cAMP, respectively (and we took $K_B = K_A$). Thus, we obtained

$$\begin{aligned}
\frac{dx}{dt} &= \beta\pi_{mar} - \delta x \\
\frac{dy}{dt} &= \pi_{mar} - \mu y \qquad\qquad (S11)\\
\pi_{mar} &= \pi_0 \frac{1+\rho(\kappa x + \kappa z + c)}{1+\kappa x + \kappa z + c} \cdot \frac{1}{1+y_0^{\;2}},
\end{aligned}$$

where MarA could be approached to a quasi-steady state ($x \propto \pi_{mar}$, a function of time). And also we had

$$\frac{y_0}{y} = \frac{1+\alpha\left([Sal]/\theta_S\right)^{\nu_S}}{1+\left([Sal]/\theta_S\right)^{\nu_S}} \,. \qquad (S12)$$

In case of maximal induction of the system with salicylate, α modulates the regulatory role of MarR. To obtain dimensional parameters, see Table S1 for values of K_R and K_A.

Analytical solutions of the model I: temporal behavior

In this section, we considered that a very strong the repressor acted on the system, MarR (i.e., $y >> 1$). We also assumed that the system was induced with high levels of salicylate, so that $y_0 = \alpha y$, and that the activation term was simply reduced to the fold change (ρ). This allowed us to simplify the model to just one ODE, given by

$$\frac{dy}{dt} \approx \frac{\pi_0 \rho}{\alpha^2 y^2} - \mu y. \qquad \text{(S13)}$$

The steady state of this ODE was $y_\infty = \left(\frac{\pi_0 \rho}{\mu \alpha^2}\right)^{1/3}$. This has the following solution (after integration by separation of variables)

$$\frac{y}{y_\infty} = \left(1 - e^{-3\mu t}\right)^{1/3}. \qquad \text{(S14)}$$

However, this analytical solution gave an over-estimation of the dynamics when solving numerically the ODE.

We then considered a situation at short times (i.e., $\alpha y << 1$) to write

$$\frac{dy}{dt} \approx \pi_0 \rho \left(1 - \alpha^2 y^2\right). \qquad \text{(S15)}$$

The steady state of this ODE was $y_\infty = \frac{1}{\alpha}$. This has the following solution (after integration by separation of variables and partial fraction decomposition)

$$\frac{y}{y_\infty} = \tanh\left(\pi_0 \rho \alpha t\right). \qquad \text{(S16)}$$

We verified with numerical simulations that this analytical solution is a good approximation for $t < t_{50}$. With this model, we calculated the response time of the system as $t_{50} = \frac{\ln(3)}{2\pi_0 \rho \alpha}$ (i.e., $y(t_{50}) = \frac{1}{2} y_\infty$).

Analytical solutions of the model II: dynamic range

Our model to describe the dynamics of a self-repressed, self-activated operon (*y*), implemented with two regulatory genes (repressor and activator), can be written as

$$\frac{dy}{dt}=\frac{\pi_0}{1+\left(\alpha_S y\right)^2}\frac{1+\rho\kappa' y}{1+\kappa' y}-\mu y, \qquad \text{(S17)}$$

where α_S describes the effect of the inducer molecule (Eq. S12), which acts on the repressor ($1 \geq \alpha_S \geq \alpha$). Here, MarA was assumed to be a stable protein ($\delta = \mu$). This assumption leads to $x = \beta y$, and does not change the dynamics of our protein of interest, MarR (*y*). This model can be solved in steady state for a strong repressor ($y >> 1$) and high activation fold ($\rho >> 1$) as

$$y_\infty \approx \left(\frac{\pi_0\rho}{\mu\alpha_S{}^2}\right)^{1/3} \propto \alpha_S{}^{-2/3}. \qquad \text{(S18)}$$

For saturating levels of salicylate, we estimated with this model an output dynamic range of $R_{\text{out}} = \alpha^{2/3}$ (i.e., the ratio between the highest and lowest values of y_∞ when varying salicylate), and an input dynamic range of $R_{\text{in}} = 9^{2/n_{in}}$ (i.e., the ratio between the salicylate values at which we have $y_\infty = \min(y_\infty) + 0.1\Delta y_\infty$ and $y_\infty = \max(y_\infty) - 0.1\Delta y_\infty$, where $\Delta y_\infty = \max(y_\infty) - \min(y_\infty)$; n_{in} is an effective Hill coefficient; see also Goldbeter & Koshland, 1981). For $\alpha = 0.05$, it turned out $R_{\text{out}} = 7.37$ and $R_{\text{in}} = 28.32$ ($n_{in} = 1.31$).

For a constitutively expressed regulator (*y*), the dynamics of its regulated operon ($\bar{y}$) can be written as

$$\frac{d\bar{y}}{dt}=\frac{\pi_0\rho}{1+\left(\alpha_S y\right)^2}-\mu\bar{y}, \qquad \text{(S19)}$$

where *y* is constant. The steady state solution for $\bar{y}$ is straightforward to obtain.

Moreover, a model to describe the dynamics of a self-repressed gene (y), with equal production rate as before, can be written as

$$\frac{dy}{dt}=\frac{\pi_0\rho}{1+\left(\alpha_S y\right)^2}-\mu y. \qquad \text{(S20)}$$

This model can be solved in steady state to obtain the same expression as before.

Finally, a model to describe the dynamics of a self-repressed gene (y) that becomes self-activator in presence of the inducer can be written as

$$\frac{dy}{dt}=\pi_0\frac{1+\rho\left(\left(1-\alpha_S\right)y\right)^2}{1+\left(\alpha_S y\right)^2+\left(\left(1-\alpha_S\right)y\right)^2}-\mu y, \qquad \text{(S21)}$$

where we have assumed competitive binding between the repressor and activator. This model can be solved in steady state, also for a strong repressor ($y >> 1$) and high activation fold ($\rho >> 1$), as

$$y_\infty \approx \frac{\pi_0\rho}{\mu}\theta\left(1-\alpha_S\right), \qquad \text{(S22)}$$

where θ is the Heaviside function.

Signal transduction and de-repression

Our model also explains why the translation rate of MarR is limited. For the repressor to work as an efficient sensor, it has to reach an appropriate concentration. First, the concentration has to be higher than the effective dissociation constant (K_R, interaction protein-DNA). In this way, the regulator can exert its repressive action on the promoter (in absence of inducer). In the case of MarR, K_R is of the order of nM (Table S1), which allows having [MarR] > K_R (lower bound). Second, at maximal concentration of inducer (*Sal*), the promoter has to be de-repressed. This imposes the condition $[\mathrm{MarR_{free}}] < K_R$. In the *marRAB* operon, the environmental molecule (antibiotic or salicylate) does not interact directly with the repressor (contrary, for example, to the *lac* operon). Instead, Cu^{2+} is responsible for MarR oxidation (Hao *et al.*, 2014), and the intracellular concentration of this cation is up to 10 μM (Rensing & Grass, 2003). This clearly imposes a maximal concentration of repressor. Knowing the oxidation curve of MarR by Cu^{2+} (Fig. S1G, and taking the effective oxidation constant as $K_{ox} \approx 1$), it turns out $[\mathrm{MarR}] < (K_R\,[Cu^{2+}]^2)^{1/3}$ (upper bound). Therefore, we propose that an inefficient translation rate of MarR might have evolved to appropriately deal with copper signaling.

Apparent transfer function and stress cross-talk

The Hill-like model $\Pi_{mar} = \dfrac{\Pi_{mar}^{\min} + \Pi_{mar}^{\max}\left([Sal]/K_S\right)^{n_S}}{1 + \left([Sal]/K_S\right)^{n_S}}$ was adjusted independently to the experimental data of induction of the wild-type and Δ*rob* systems, obtaining the corresponding apparent transfer functions ([*Sal*] is the concentration of salicylate in mM). We got $\Pi_{mar}^{\min}$ = 2,260 (+/- 746) AU, $\Pi_{mar}^{\max}$ = 20,000 AU (fixed), K_S = 0.88 (+/- 0.12) mM, and n_S = 1.28 (+/- 0.19) for the wild-type system, and $\Pi_{mar}^{\min}$ = 1,089 (+/- 1011) AU, $\Pi_{mar}^{\max}$ = 12,500 AU (fixed), K_S = 0.72 (+/- 0.19) mM, and n_S = 1.45 (+/- 0.48) for the Δ*rob* system. With the inferred sigmoidal models, we calculated the input and output dynamic ranges: R_{in} = 20 - 30 and R_{out} = 9 - 11 for both systems.

Apart from salicylate, the *marRAB* operon can also be induced by CRP-cAMP. We predicted computationally and verified experimentally the two-dimensional transfer function of the system. Then, we defined a degree of stress-cross talk as $\left|\dfrac{[YFP]_\infty|_{cAMP}}{[YFP]_\infty|_{cAMP=0}} - 1\right|$.

Stochastic modeling

Using a Langevin approach, our ODE-based mathematical model can be extended to account for the inherent stochasticity of biological systems. Because in bacteria noise has two components (intrinsic and extrinsic) and is predominantly generated at the transcription level (Swain *et al.*, 2002), we considered a stochastic process ξ_μ (where μ is the inverse of the correlation time) with statistics $\left\langle \xi_\mu(t) \right\rangle = 0$ and $\left\langle \xi_\mu(t')\xi_\mu(t'+t) \right\rangle = \frac{\mu}{2} e^{-\mu|t|}$. Thus, and having assumed similar mRNA degradation and MarR translation rates, we can write

$$\begin{aligned} \frac{dx}{dt} &= \beta\pi_{mar} - \delta x + \beta\sqrt{\frac{2\pi_{mar}}{K_R}}\xi_\delta(t) + \beta q \xi_\mu(t) \\ \frac{dy}{dt} &= \pi_{mar} - \mu y + \sqrt{\frac{2\pi_{mar}}{K_R}}\xi_\delta(t) + q\xi_\mu(t) \end{aligned} , \qquad \text{(S23)}$$

where q is the extrinsic noise magnitude. This system can be solved numerically by following the method described by Rodrigo *et al.* (2011).

Note on the potential excitability of the system

The regulatory architecture of the *marRAB* operon is suitable to present excitable behavior (even to produce sustained oscillations) in the non-induced state, due to the interlinked, delay-based positive and negative feedbacks (Hasty *et al.*, 2002; Guantes & Poyatos, 2006). For this architecture, oscillations appear when a clear separation of time scales between activator and repressor dynamics exists. This implies two conditions: *i*) the activator degradation should be stronger than the repressor one (in our case, MarA is quickly degraded by a protease, whereas MarR is diluted due to cell growth rate), and *ii*) the activator translation rate should be also stronger than the repressor one (here, the RBS of MarA is stronger than the one of MarR). However, in the *mar* system, the activator (MarA) works as a monomer, which prevents this behavior even having much faster dynamics (see in Fig. S5B how oscillations arise when high cooperativity is introduced for both regulators). Moreover, when competitive binding between MarA and MarR (in particular, that MarA prevents MarR binding; Garcia-Bernardo & Dunlop, 2013) is considered, stochastic pulses can appear, even with a monomeric activator (Fig. S5E). However, previous experiments support relatively independent action of MarA and MarR (Martin & Rosner, 1997), aside from their operators do not overlap. Furthermore, in our single cell experiments without salicylate, we did not observe pulses in YFP, neither with our predictive model.

Supplementary Figures and Figure Legends

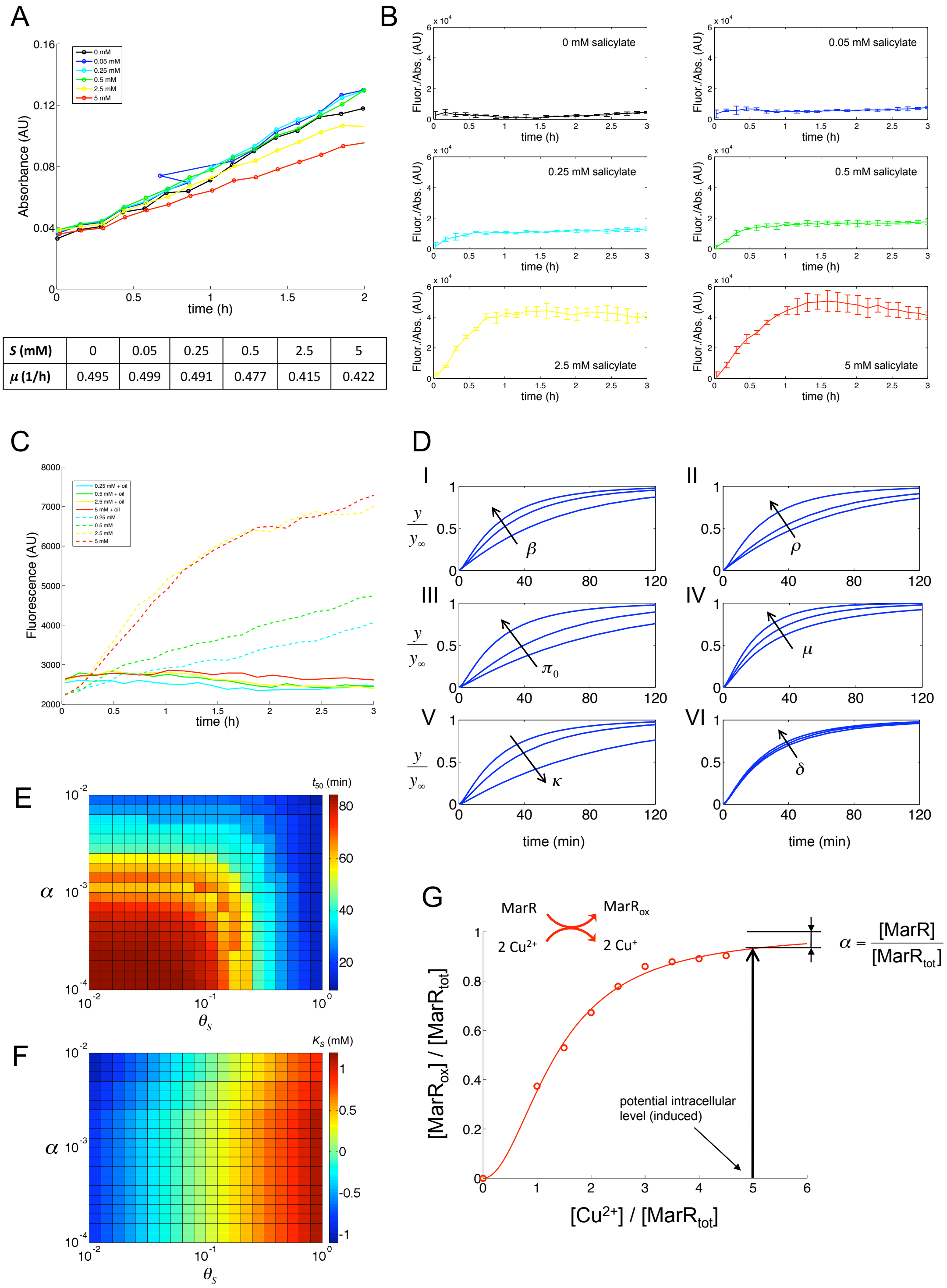

S (mM)	0	0.05	0.25	0.5	2.5	5
μ (1/h)	0.495	0.499	0.491	0.477	0.415	0.422

Figure S1: Experimental and computational results of the dynamic behavior of the system (associated to Figure 1).

(A) Effect of the salicylate concentration in the growth rate of the cells (wild-type system, strain IE01). Absorbance values are averages of replicates.

(B) Dynamic response of the system upon induction with different concentrations of salicylate (wild-type system). We represent the normalized fluorescence (YFP) with time. Error bars represent standard deviations.

(C) Dynamic response of the wild-type system upon induction with different concentrations of salicylate in aerobic (dashed lines) and anaerobic (solid lines) conditions. We represent the absolute fluorescence (YFP) with time. Fluorescence values are averages of replicates. Anaerobic conditions were achieved by using mineral oil to cover the cultures. The no expression of the *mar* circuit with salicylate under anaerobic conditions may be explained, at least in part, by the fact that copper appears to shift intracellularly from Cu^{2+} to Cu^{+} in absence of oxygen (Rensing & Grass, 2003).

(D) Computational simulations of the dynamic behavior with toy parameter values. Model-based sensitivity analysis of various parameters. (I) $\beta = 30 / 10 / 1$. (II) $\rho = 5 / 2 / 1$. (III) $\pi_0 = 1 / 0.4 / 0.2$ min^{-1}. (IV) $\mu = 0.02 / 0.01 / 0.005$ min^{-1}. (V) $\kappa = 0.01 / 0.02 / 0.1$. (VI) $\delta = 0.5 / 0.1 / 0.01$ min^{-1}. For parameters not specified, we took the following parameter values: $\delta = 0.5$ min^{-1}, $\mu = 0.01$ min^{-1}, $\pi_0 = 1$ min^{-1}, $\rho = 5$, $\kappa = 0.01$, $\beta = 30$, $z = c = 0$, $\theta_S = 0.1$ mM, $\nu_S = 2$, and $\alpha = 0.01$.

(E, F) Simulations to study the effect of θ_S and α on (E) response time, calculated as the time to reach the 50% of the steady state value (t_{50}) upon induction with [*Sal*] = 5 mM, and (F) half maximal effective concentration of salicylate (K_S). We took the same parameter values as before. These plots show that when α approaches to 0 the response time increases because of the lack of active repressor in the cell. In the limit (α = 0), for [*Sal*] >> θ_S, the situation will be like a gene without autogenous regulation. However, this is not what we observe experimentally, which leads us to consider a non-negligible value of α (e.g., $\alpha = 0.01$). The plots also show that θ_S is the primary parameter responsible of changing K_S, although K_S can also be influenced by α in certain regime (e.g., $0.001 < \alpha < 0.01$).

(G) Transfer function of copper regulation relating the fraction of oxidized MarR ($\mathrm{MarR_{ox}}$) with the relative amount of $\mathrm{Cu^{2+}}$. Experimental values (small circles, data taken from Hao *et al.*, 2014) represent averages of replicates of the relative to the maximum oxidation. The line corresponds to $\dfrac{\left(\dfrac{[\mathrm{Cu^{2+}}]}{[\mathrm{MarR_{tot}}]}\right)^2}{K_{\mathrm{ox}}^2+\left(\dfrac{[\mathrm{Cu^{2+}}]}{[\mathrm{MarR_{tot}}]}\right)^2}$, fitted with K_{ox} = 1.35. At first order, we have $\alpha \approx \left(K_{\mathrm{ox}}\dfrac{[\mathrm{MarR_{tot}}]}{[\mathrm{Cu^{2+}}]}\right)^2$. The intracellular copper levels upon induction with salicylate may be about 10 μM (Rensing & Grass, 2003), and the concentration of MarR about 2 μM (Martin & Rosner, 2004). This gives $\alpha \approx 5\%$.

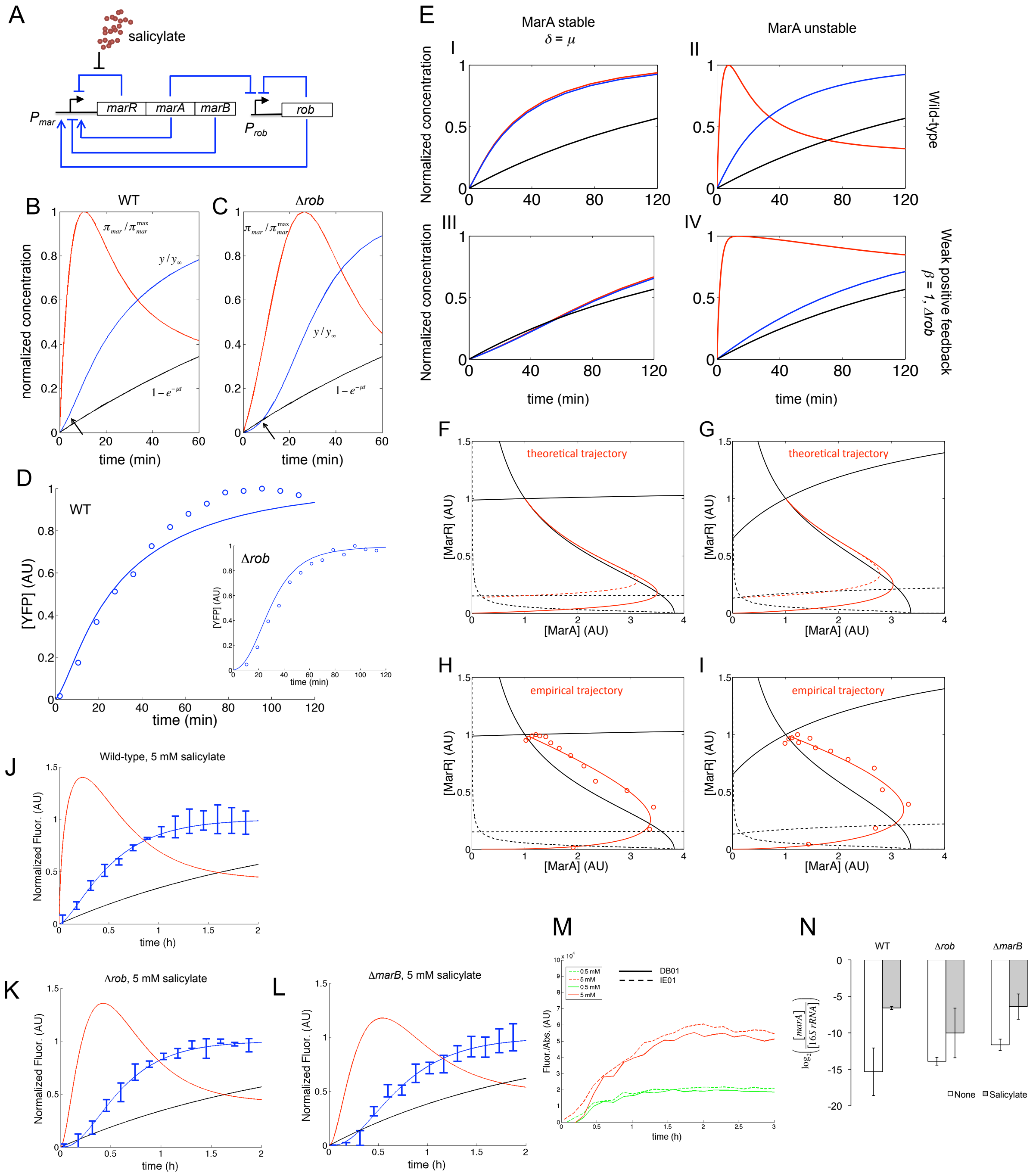
A
salicylate
P_{mar}
marR
marA
marB
P_{rob}
rob
B
WT
normalized concentration
$\pi_{mar}/\pi_{mar}^{max}$
y/y_∞
$1-e^{-\mu t}$
time (min)
C
Δrob
D
[YFP] (AU)
WT
Δrob
time (min)
E
MarA stable
$\delta = \mu$
MarA unstable
I
II
III
IV
Normalized concentration
Wild-type
Weak positive feedback
$\beta = 1$, Δrob
time (min)
F
G
theoretical trajectory
[MarR] (AU)
[MarA] (AU)
H
I
empirical trajectory
J
Wild-type, 5 mM salicylate
Normalized Fluor. (AU)
time (h)
K
Δrob, 5 mM salicylate
L
ΔmarB, 5 mM salicylate
M
Fluor./Abs. (AU)
0.5 mM
5 mM
DB01
IE01
time (h)
N
WT
Δrob
ΔmarB
$\log_2\left(\frac{[marA]}{[16S\ rRNA]}\right)$
None
Salicylate

Figure S2: Experimental results and computational simulations of the dynamic response including *rob* and *marB* genes (associated to Figure 2).

(A) Scheme of the natural circuit where MarR, MarA, MarB and Rob regulate the *marRAB* promoter.

(B - D) Model predictions of the dynamic response (simulations to study the effect of Rob). (B) $z = 100$ simulates the wild-type system, and (C) $z = 0$ the Δ*rob* system. The arrows mark different response abilities at short times (blue curves). (D) Simulations (solid lines) together with gene expression experimental data (circles). We took the parameter values shown in Table S1.

(E) Simulations to analyze the dynamics of the system for stable or unstable MarA (parameter δ) and efficient or inefficient positive feedback (parameter β). MarR in blue, MarA in red. Black line corresponds to growth-rate-based exponential curve, $\left(1-e^{-\mu t}\right)$. We took the same parameter values as before.

(F - I) Nullclines of the system (phase diagram). Solid black lines correspond to nullclines at 5 mM salicylate, and dashed black lines to nullclines without salicylate. (F, H) Wild-type system. (G, H) Δ*rob* system. (F, G) Theoretical trajectories (solid red curves for simulations starting from the origin; dashed red curves from the equilibrium point in absense of salicylate). (H, I) Representation of the normalized fluorescence (YFP, a measure of MarR) and the inferred promoter activity (a measure of MarA) with time in the phase space (red circles), together with the empirical trajectory calculated with Eqs. (S2) and (S3) (red line). The concentrations of MarA and MarR were normalized by the steady state values at 5 mM salicylate.

(J - L) Normalized dynamic response upon induction with 5 mM salicylate of (J) the wild-type system (strain IE01), (K) the Δ*rob* system (strain IE02), and (L) the Δ*marB* system (strain DB01). Error bars correspond to experimental data, whereas the blue and black lines to different exponential models, $\left(1-e^{-\lambda t}\right)^{m}$ and $\left(1-e^{-\mu t}\right)$ respectively. The red line corresponds to promoter activity calculated with the best-fit exponential model. Fluorescence values are normalized by the maximum to compare curves. The boost time of the system (τ) here was defined when promoter activity is maximal, Eq. (S5). We obtained the following parameter values: (J) $\lambda = 2.42$ h^{-1}, $m = 1.66$, $\mu = 0.42$ h^{-1}, and $\tau = 0.23$ h; (K) $\lambda = 2.81$ h^{-1}, $m = 2.99$, $\mu = 0.43$ h^{-1}, and $\tau = 0.42$ h; and (L) $\lambda = 2.28$ h^{-1}, $m = 2.92$, $\mu = 0.48$ h^{-1}, and $\tau = 0.54$ h.

(M) Dynamic response of the Δ*marB* system upon induction with different concentrations of salicylate. Dynamics shown with solid lines correspond to the Δ*marB* system, whereas dynamics shown with dashed lines correspond to the wild-type system. In both cases, we represent the normalized fluorescence (YFP) with time. Fluorescence values are averages of replicates.

(N) Characterization by qRT-PCR of the intracellular RNA concentration of gene *marA* for different strains (wild-type, Δ*rob*, and Δ*marB*), with (5 mM) and without salicylate. We report the ratio between the expression of gene *marA* and a constitutive housekeeping gene (16S ribosomal RNA, rRNA). Error bars correspond to standard deviations.

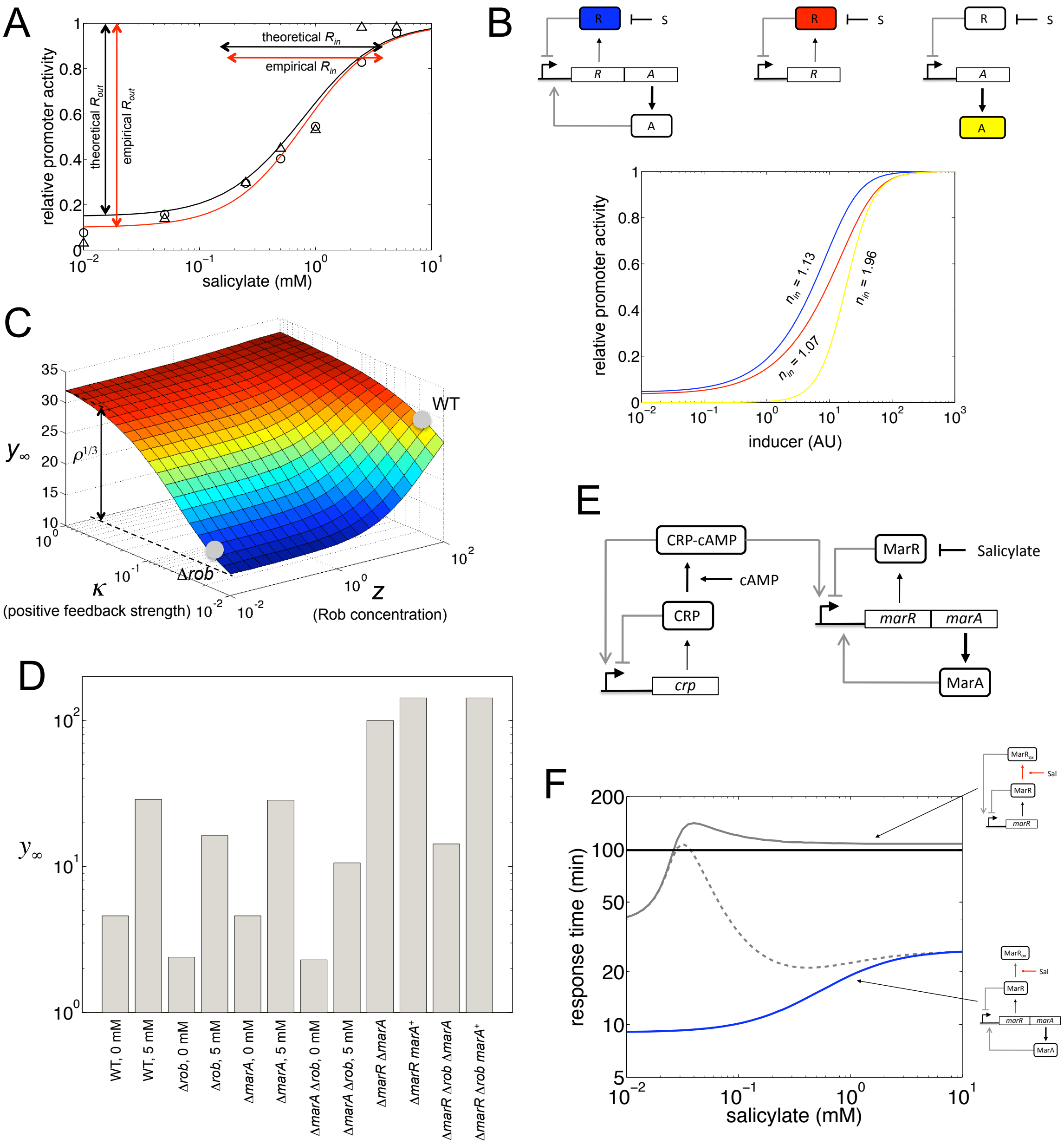
A
relative promoter activity
salicylate (mM)
theoretical R_{in}
empirical R_{in}
theoretical R_{out}
empirical R_{out}
0
0.2
0.4
0.6
0.8
1
10^{-2}
10^{-1}
10^{0}
10^{1}
B
R
A
S
relative promoter activity
inducer (AU)
n_{in} = 1.13
n_{in} = 1.07
n_{in} = 1.96
10^{-2}
10^{-1}
10^{0}
10^{1}
10^{2}
10^{3}
C
y_∞
$\rho^{1/3}$
WT
Δrob
κ
(positive feedback strength)
z
(Rob concentration)
10
15
20
25
30
35
10^{0}
10^{-1}
10^{-2}
10^{0}
10^{2}
D
y_∞
10^{0}
10^{1}
10^{2}
WT, 0 mM
WT, 5 mM
Δrob, 0 mM
Δrob, 5 mM
ΔmarA, 0 mM
ΔmarA, 5 mM
ΔmarA Δrob, 0 mM
ΔmarA Δrob, 5 mM
ΔmarR ΔmarA
ΔmarR $marA^+$
ΔmarR Δrob ΔmarA
ΔmarR Δrob $marA^+$
E
CRP-cAMP
cAMP
CRP
crp
MarR
Salicylate
marR
marA
MarA
F
response time (min)
salicylate (mM)
5
10
20
50
100
200
10^{-2}
10^{-1}
10^{0}
10^{1}
$MarR_{ox}$
Sal
MarR
marR
marA
MarA

Figure S3: Experimental results and computational simulations of the dynamic range and response time (associated to Figure 3).

(A) Model prediction of the transfer function of the system. Relative promoter activity (in steady state) of the system as a function of salicylate. Solid black line represents model simulations, whereas circles (wild-type) and triangles (Δrob) are experimental data. We took the parameter values shown in Table S1. In addition, the Hill-like model $\Pi_{mar} = \frac{\Pi_{mar}^{\min} + \left([Sal]/K_S\right)^{n_S}}{1 + \left([Sal]/K_S\right)^{n_S}}$ adjusted to all experimental data (from wild-type and Δrob systems; red line), gave $\Pi_{mar}^{\min}$ = 0.10 (+/- 0.04), K_S = 0.79 (+/- 0.10) mM, and n_S = 1.36 (+/- 0.21). The plot shows comparatively theoretical and empirical values of input and output dynamic ranges.

(B) Model predictions of the transfer functions of various control systems. We represent the relative promoter activity (in steady state) of the system as a function of the inducer. The blue curve corresponds to the wild-type *mar* circuit, whereas the red curve corresponds to a sensor gene negatively autoregulated and the yellow curve to a sensor gene constitutively expressed. For simplicity, here we took $v_S = 1$ and $\alpha = 0$. The rest of parameter values are from Table S1.

(C) The positive feedback strength (parameter κ) and Rob concentration (parameter z) modulate the steady state of the system (simulations for 5 mM salicylate). Despite, the output dynamic range is almost constant.

(D) Model predictions for different conditions (genotypes and salicylate levels). The predictions show $\pi_{mar}(5\text{ mM})/\pi_{mar}(0\text{ mM})|_{\mathrm{WT}} \approx \pi_{mar}(5\text{ mM})/\pi_{mar}(0\text{ mM})|_{rob} \approx \alpha^{2/3} =$ 7.3, and $\pi_{mar}(5\text{ mM})/\pi_{mar}(0\text{ mM})|_{marA} \approx \rho = 10$. In addition, they show

$\pi_{mar}(\mathrm{WT})/\pi_{mar}(rob)|_{0\ \mathrm{mM}} \approx \pi_{mar}(\mathrm{WT})/\pi_{mar}(rob)|_{5\ \mathrm{mM}} \approx \rho^{1/3} \approx 2$. Finally, they show $\pi_{mar}(marA^{+})/\pi_{mar}(marA)|_{marR} \approx 1.4$, and $\pi_{mar}(marA^{+})/\pi_{mar}(marA)|_{marR,\ rob} \approx \rho = 10$. These predictions are in tune with previous experimental results (Martin & Rosner, 1997).

(E) Scheme of the coupled dual autogenous regulatory systems by CRP and MarR-MarA in the bacterial genome. The implementations are different each other.

(F) Simulations to analyze the response time of two implementations of the dual autogenous control system. The blue curve corresponds to the wild-type *mar* circuit. The gray curves correspond to a hypothetical situation where the oxidized MarR acts as an activator. Solid gray curve for competitive binding between the repressor and activator, and dashed gray curve for independent binding. Parameter values from Table S1.

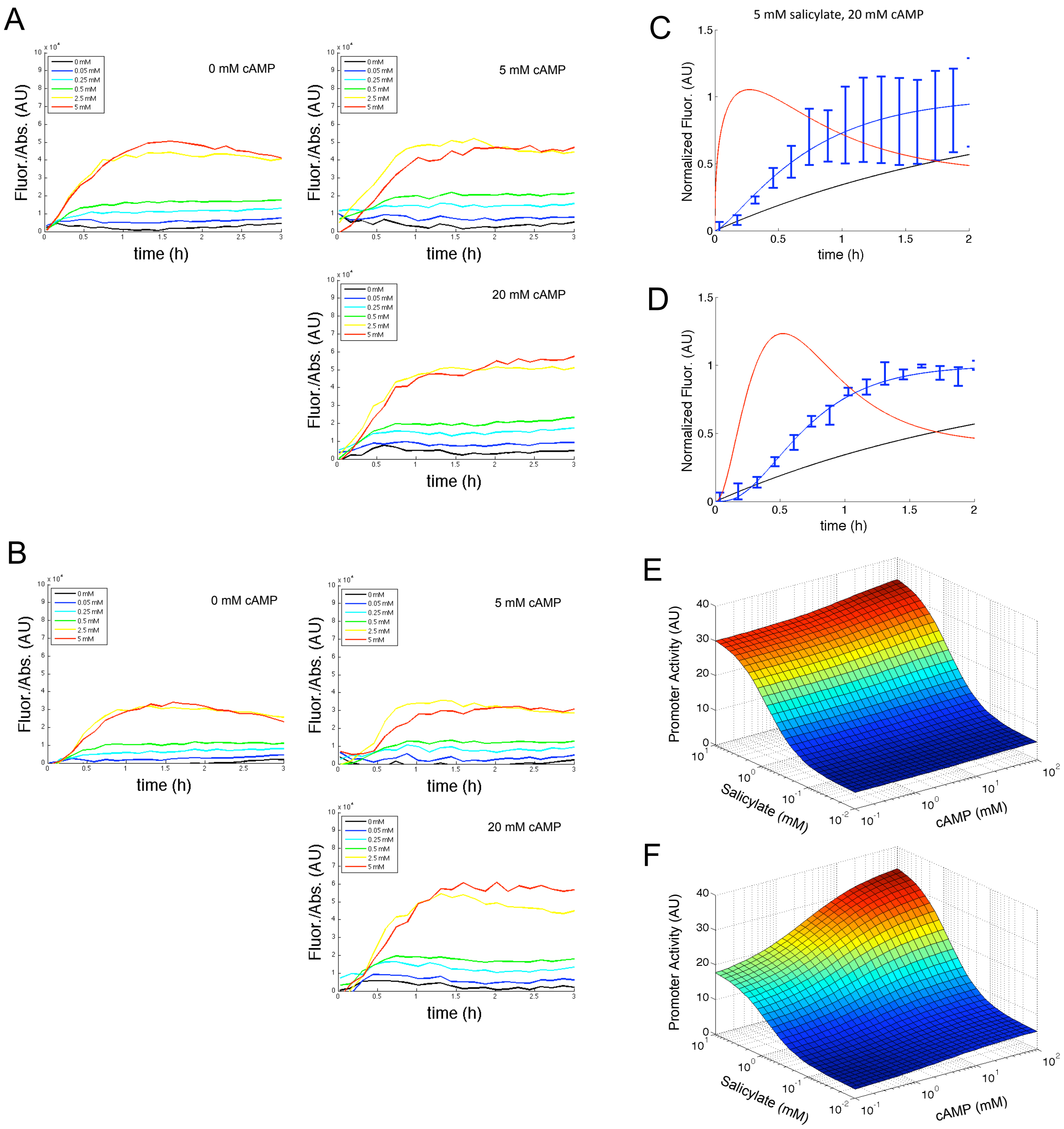
A
0 mM cAMP
5 mM cAMP
20 mM cAMP
Fluor./Abs. (AU)
time (h)
x 10^4
0 mM
0.05 mM
0.25 mM
0.5 mM
2.5 mM
5 mM
B
0 mM cAMP
5 mM cAMP
20 mM cAMP
Fluor./Abs. (AU)
time (h)
C
5 mM salicylate, 20 mM cAMP
Normalized Fluor. (AU)
time (h)
D
Normalized Fluor. (AU)
time (h)
E
Promoter Activity (AU)
Salicylate (mM)
cAMP (mM)
F
Promoter Activity (AU)
Salicylate (mM)
cAMP (mM)

Figure S4: Experimental results and computational simulations on the *marRAB* promoter integration of salicylate and cAMP signals (associated to Figure 4).

(A, B) Dynamic response of the system upon induction with different concentrations of salicylate and cAMP. (A) Wild-type system (strain IE01). (B) Δ*rob* system (strain IE02). We represent the normalized fluorescence (YFP) with time. Fluorescence values are averages of replicates.

(C, D) Normalized dynamic response of the wild-type system (C) and the Δ*rob* system (D) upon induction with 5 mM salicylate and 20 mM cAMP. Error bars correspond to experimental data (we repeated the experiment of induction for the wild-type system different times, but we always obtained high variability between clones), whereas the blue and black lines to different exponential models, $\left(1-e^{-\lambda t}\right)^m$ and $\left(1-e^{-\mu t}\right)$ respectively. The red line corresponds to promoter activity calculated with the best-fit exponential model. Fluorescence values are normalized by the maximum to compare curves. For the wild-type system, we got $\lambda = 1.60$ h^{-1}, $m = 1.40$ and $\mu = 0.36$ h^{-1}, and for the Δ*rob* system, $\lambda = 2.50$ h^{-1}, $m = 3.23$ and $\mu = 0.43$ h^{-1}. The boost time of the system (τ), here defined when promoter activity is maximal, Eq. (S5), was $\tau = 0.26$ h for the wild-type system, and $\tau = 0.52$ h for the Δ*rob* system.

(E, F) Model-based predictions of the transfer function of the system as a function of the two input signals, salicylate and cAMP. (E) Wild-type system. (F) Δ*rob* system. For this plot, we used the parameter values shown in Table S1.

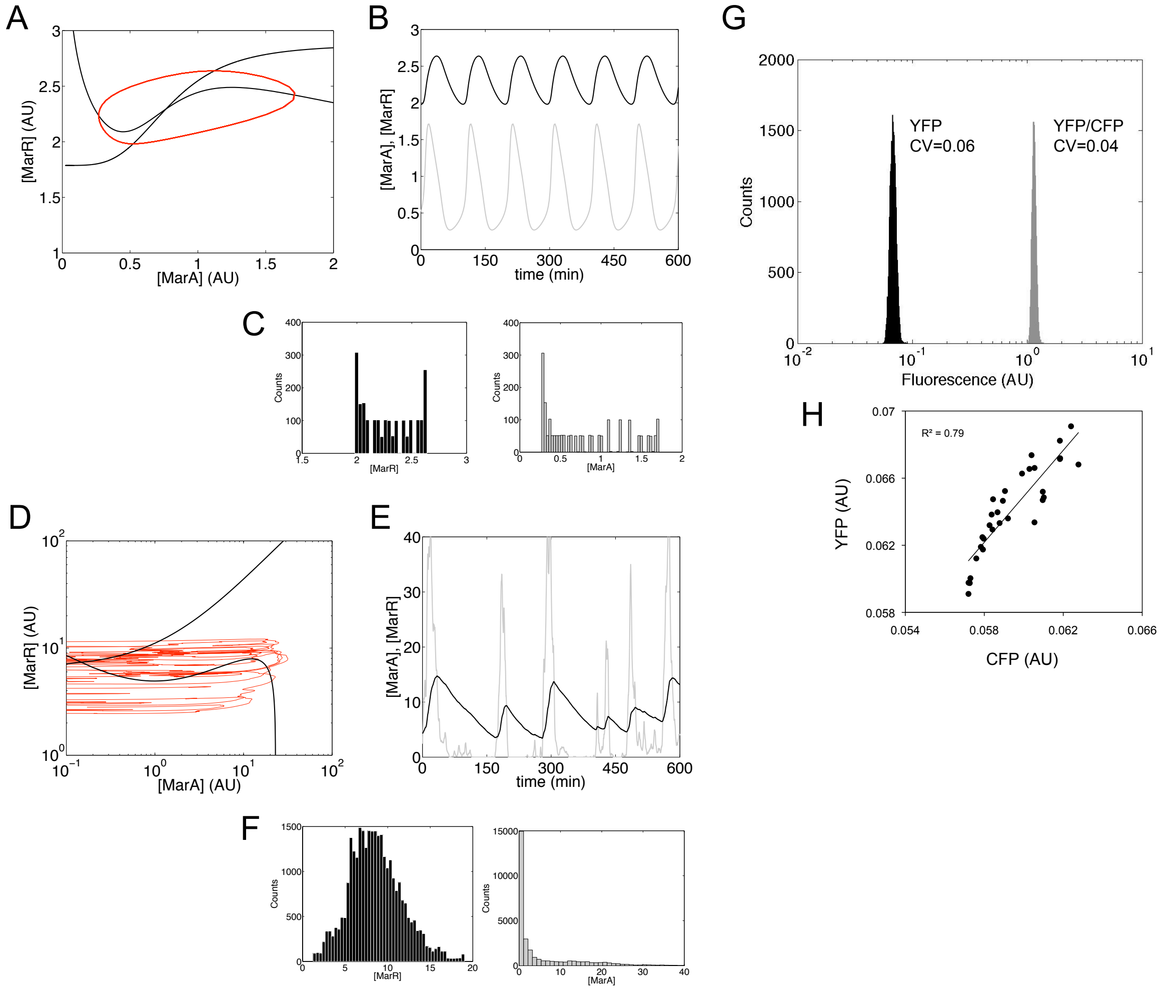
A
[MarR] (AU)
[MarA] (AU)
B
[MarA], [MarR]
time (min)
C
Counts
[MarR]
[MarA]
D
[MarR] (AU)
[MarA] (AU)
E
[MarA], [MarR]
time (min)
F
Counts
[MarR]
[MarA]
G
Counts
YFP
CV=0.06
YFP/CFP
CV=0.04
Fluorescence (AU)
H
R² = 0.79
YFP (AU)
CFP (AU)

Figure S5: Theoretical analysis of the non-induced dynamic response (associated to Figures 5).

(A - C) Phase diagram of the system in absence of salicylate showing an oscillatory pattern when MarA is cooperative (A). Here, we assumed high cooperativity (Hill coefficient of 4) for both MarA and MarR. The black lines correspond to the nullclines, with a different shape than for the wild-type system. The red curve represents a deterministic trajectory. The dynamics is represented with time in (B), where MarA is shown in gray and MarR in black. In (C) we show the resulting distributions of expression. For these plots, we took the following parameter values: $\delta = 0.15$ min^{-1}, $\mu = 0.01$ min^{-1}, $\pi_0 = 0.2$ min^{-1}, $\rho = 10$, $\kappa = 1$, $\beta = 5$, and $z = c = 0$.

(D - F) Phase diagram of the system in absence of salicylate showing stochastic pulses when MarA prevents MarR binding (D). To model this hypothetical competitive binding between MarA and MarR, we replaced y_0 in Eqs. (S11) by $y_0/(1+x)$. The black lines correspond to the nullclines, with a different shape than for the wild-type system. The red curve represents a stochastic trajectory. The dynamics is represented with time in (E), where MarA is shown in gray and MarR in black. In (F) we show the resulting distributions of expression. For these plots, we took the parameter values shown in Table S1, with $z = 0$.

(G) Comparison of the distributions YFP and YFP/CFP for all single cells at all time points. The coefficient of variation (CV) is lower in case of YFP/CFP.

(H) Scatter plot between YFP and CFP for a single cell trajectory showing a good correlation (dominance of extrinsic noise).

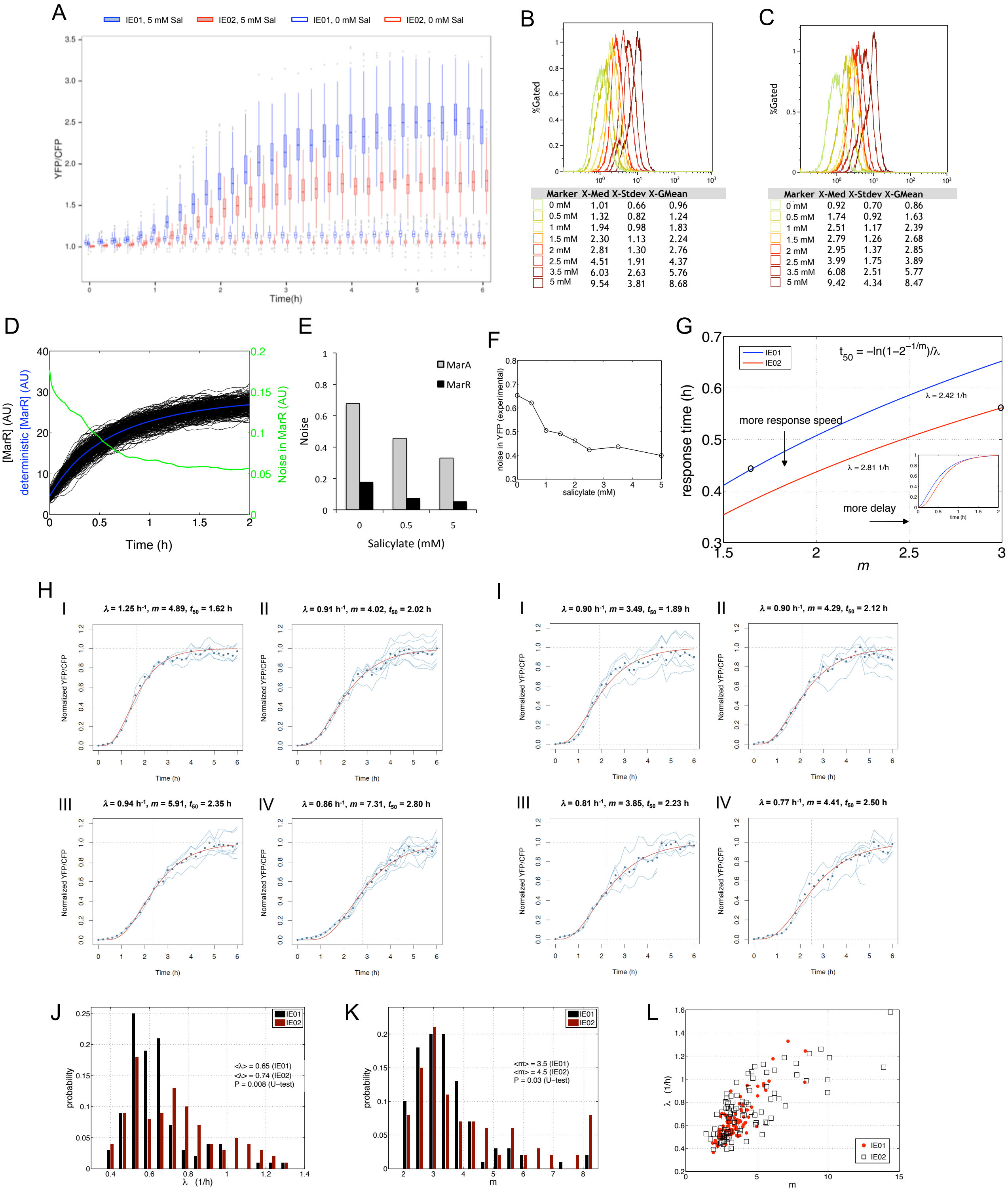

B

Marker	X-Med	X-Stdev	X-GMean
0 mM	1.01	0.66	0.96
0.5 mM	1.32	0.82	1.24
1 mM	1.94	0.98	1.83
1.5 mM	2.30	1.13	2.24
2 mM	2.81	1.30	2.76
2.5 mM	4.51	1.91	4.37
3.5 mM	6.03	2.63	5.76
5 mM	9.54	3.81	8.68

C

Marker	X-Med	X-Stdev	X-GMean
0 mM	0.92	0.70	0.86
0.5 mM	1.74	0.92	1.63
1 mM	2.51	1.17	2.39
1.5 mM	2.79	1.26	2.68
2 mM	2.95	1.37	2.85
2.5 mM	3.99	1.75	3.89
3.5 mM	6.08	2.51	5.77
5 mM	9.42	4.34	8.47

Figure S6: Experimental results of the dynamic response upon induction with salicylate at the single cell level (associated to Figure 6).

(A) Box plot of the dynamic response (using YFP/CFP intensity) of multiple single cells for the wild-type system (strain IE01) and the Δ*rob* system (strain IE02). We present results for non-induced and induced (5 mM salicylate) cells.

(B, C) Flow cytometry analysis (using YFP intensity) of the (B) wild-type and (C) Δ*rob* systems, for several conditions of salicylate.

(D) Model simulations to study the stochastic response. Different trajectories (simulating different single cells) are shown in black. In green, we represent noise in gene expression (coefficient of variation). In blue, we show the dynamics in the deterministic regime (which approximates very well to the average).

(E) Model predictions of noise in expression of MarA (η_x, gray bars) and MarR (η_y, black bars) as a function of salicylate.

(F) Experimental noise calculated with flow cytometry data, for the wild-type system, to validate the results reported in (E).

(G) Map of the response time, which is determined by *i*) the time lag to react (empirical parameter *m*), and *ii*) the speed at which the expression increases (empirical parameter λ). Open circles correspond the biological systems. The inset shows the experimentally determined dynamics.

(H, I) Monitoring of fluorescence with time of four representative lineages showing different response times. (H) Wild-type system. (I) Δ*rob* system.

(J, K) Distributions of the empirical parameters λ and m, obtained by fitting the exponential model $\left(1-e^{-\lambda t}\right)^{m}$ to the single cell trajectories of 100 lineages. Black bars correspond to the wild-type system, and red ones to the Δ*rob* system. λ and m are significantly higher in the Δ*rob* system ($P < 0.05$, *U*-test).

(L) Scatter plot of λ and m [data from (J, K)] showing higher variability in case of the Δ*rob* system.

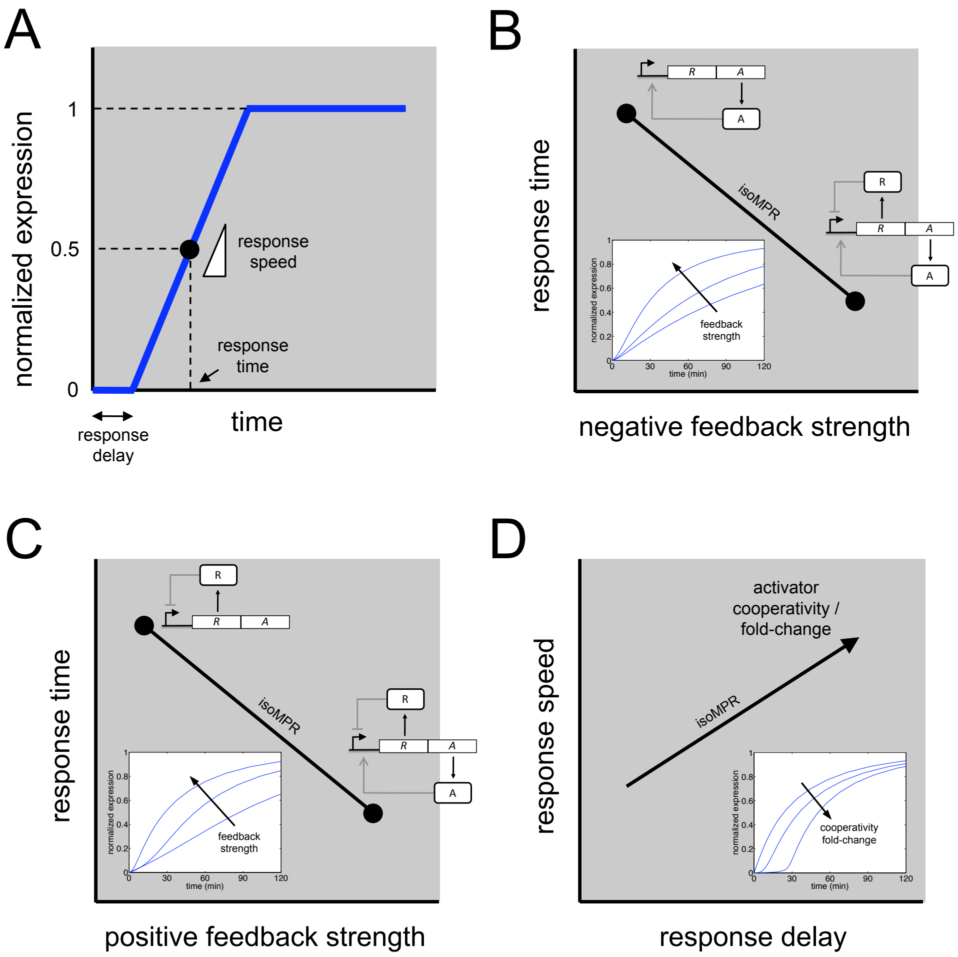
A
normalized expression
1
0.5
0
response speed
response time
response delay
time
B
response time
R
A
A
isoMPR
R
R
A
A
normalized expression
feedback strength
time (min)
negative feedback strength
C
response time
R
R
A
isoMPR
R
R
A
A
normalized expression
feedback strength
time (min)
positive feedback strength
D
response speed
activator cooperativity / fold-change
isoMPR
normalized expression
cooperativity fold-change
time (min)
response delay

Figure S7: Analysis of the dynamic response of a circuit with dual autogenous regulation.

(A) Scheme of the dynamic response.

(B) The response time depends with a decreasing trend on the negative feedback strength (understood as the binding affinity of the repressor to the promoter), being constant the maximal production rate of the operon (isoMPR). The inset shows model simulations.

(C) The response time depends with a decreasing trend on the positive feedback strength (understood as the binding affinity of the activator to the promoter). The inset shows model simulations.

(D) The response speed and response delay are positively correlated and they depend with an increasing trend on the degree of multimerization of the activator (cooperativity) and its ability to stimulate of RNA polymerase (fold-change). The inset shows model simulations.

Supplementary Tables

Table S1: Nominal parameter values for the mathematical model.

Parameter	Value	Note	Reference
δ	0.5 min^{-1}	Protein half-life of ~1 min.	Griffith *et al.*, 2004
μ	0.007 – 0.01 min^{-1}	-	This work
π_0	0.1 min^{-1}	Assuming transcription rate of ~1 nM/min, translation rate of ~0.05-0.1 min^{-1}, and mRNA degradation rate of ~0.1 min^{-1}	Levine *et al.*, 2007
β	30	With RBS calculator	Salis *et al.*, 2009
ρ	10	Experimental data show ~6-fold increase in expression due to the direct effect of MarA.	Martin *et al.*, 1996 Chubiz *et al.*, 2012
κ	0.02	Having K_A = 1000-1500 nM and K_R = 5-10 nM (as $\kappa = K_R / K_A$)	Martin *et al.*, 2008 Seoane *et al.*, 1995
θ_S	0.13 mM	Adjusted to get the experimental transfer function. Estimated from $K_S \approx 0.9$ mM, knowing that $\theta_S \approx K_S\,(2\alpha)^{1/\nu_S}$	Cohen *et al.*, 1993
ν_S	1.4	-	This work
α	0.05	Assuming $[Cu^{2+}] / [MarR] \approx 5$ upon induction with 5 mM salicylate	Hao *et al.*, 2014
z	100	The number of Rob molecules per cell is ~10,000, but they aggregate and are inactive. The fraction that is free is assumed ~10%	Griffith *et al.*, 2009
K_C	5 mM	-	Setty *et al.*, 2003
q	0.3	Knowing that $q = \eta_{ex}\,\pi_{\text{mar}}\,(2/\mu)^{1/2}$	Swain *et al.*, 2002

Table S2: *E. coli* operons with dual autogenous regulation[5,6] from RegulonDB (Salgado *et al*., 2013).

Regulator	Operon	Note	Molecular implementation
ChbR	*chbBCARFG*	Repressor that becomes activator in response to chitobiose. AraC/XylS family of transcriptional regulators.	Multifunctional regulator
CRP	*crp*	Repressor that becomes activator in response to cAMP. CRP-FNR superfamily of transcription factors.	Multifunctional regulator
LldR	*lldPRD*	Repressor that becomes activator in response to lactate. GntR family of transcriptional regulators.	Multifunctional regulator
MarR, MarA	*marRAB*	Control of multiple antibiotic resistance. AraC/XylS family of transcriptional regulators.	Distributed regulation

---

[5] The operons with dual regulators (according to RegulonDB) *ada-alkB*, *araC*, *dnaAN-recF*, *gadAXW*, *leuO*, *melR*, *murR*, and *phoPQ* are not considered as systems with dual autogenous control in the sense of our study.

[6] AraC or MelR, also transcriptional regulators of the AraC/XylS family, repress their own expression, whereas they exert dual regulation (with arabinose or melibiose as inducers) on their targets.

Supplementary References

Alekshun MN, Levy SB (1997) Regulation of chromosomally mediated multiple antibiotic resistance: the mar regulon. *Antimicrob Agents Chemother* 41: 2067-2075.

Baba T, Ara T, Hasegawa M, Takai Y, Okumura Y, Baba M, Datsenko KA, Tomita M, Wanner BL, Mori H (2006) Construction of Escherichia coli K-12 in-frame, single-gene knockout mutants: the Keio collection. *Mol Syst Biol* 2: 2006.0008.

Bintu L, Buchler NE, Garcia HG, Gerland U, Hwa T, Kondev J, Phillips R (2005) Transcriptional regulation by the numbers: models. *Curr Opin Genet Dev* 15: 116-124.

Carothers JM, Goler JA, Juminaga D, Keasling JD (2011) Model-driven engineering of RNA devices to quantitatively program gene expression. *Science* 334: 1716-1719.

Chubiz LM, Glekas GD, Rao CV (2012) Transcriptional cross talk within the mar-sox-rob regulon in Escherichia coli is limited to the rob and marRAB operons. *J Bacteriol* 194: 4867-4875.

Cohen SP, Levy SB, Foulds J, Rosner JL (1993) Salicylate induction of antibiotic resistance in Escherichia coli: activation of the mar operon and a mar-independent pathway. *J Bacteriol* 175: 7856-7862.

Datsenko KA, Wanner BL (2000) One-step inactivation of chromosomal genes in Escherichia coli K-12 using PCR products. *Proc Natl Acad Sci USA* 97: 6640-6645.

Garcia-Bernardo J, Dunlop MJ (2013) Tunable stochastic pulsing in the Escherichia coli multiple antibiotic resistance network from interlinked positive and negative feedback loops. *PLoS Comput Biol* 9: e1003229.

Goldbeter A, Koshland DE Jr (1981) An amplified sensitivity arising from covalent modification in biological systems. *Proc Natl Acad Sci USA* 78: 6840-6844.

Griffith KL, Shah IM, Wolf RE (2004) Proteolytic degradation of Escherichia coli transcription activators SoxS and MarA as the mechanism for reversing the induction of the superoxide (SoxRS) and multiple antibiotic resistance (Mar) regulons. *Mol Microbiol* 51: 1801-1816.

Griffith KL, Fitzpatrick MM, Keen EF III, Wolf RE Jr (2009) Two functions of the C-terminal domain of Escherichia coli Rob: mediating “sequestration-dispersal” as a novel off-on switch for regulating Rob’s activity as a transcription activator and preventing degradation of Rob by Lon protease. *J Mol Biol* 388: 415-430.

Guantes R, Poyatos JF (2006) Dynamical principles of two-component genetic oscillators. *PLoS Comput Biol* 2: e30.

Hasty J, Dolnik M, Rottschäfer V, Collins JJ (2002) Synthetic gene network for entraining and amplifying cellular oscillations. *Phys Rev Lett* 88: 148101.

Hao Z, Lou H, Zhu R, Zhu J, Zhang D, Zhao BS, Zeng S, Chen X, Chan J, He C, Chen PR (2014) The multiple antibiotic resistance regulator MarR is a copper sensor in Escherichia coli. *Nat Chem Biol* 10: 21-28.

Levine E, Zhang Z, Kuhlman T, Hwa T (2007) Quantitative characteristics of gene regulation by small RNA. *PLoS Biol* 5: e229.

Martin RG, Jair KW, Wolf RE Jr, Rosner JL (1996) Autoactivation of the marRAB multiple antibiotic resistance operon by the MarA transcriptional activator in Escherichia coli. *J Bacteriol* 178: 2216-2223.

Martin RG, Rosner JL (1997) Fis, an accessorial factor for transcriptional activation of the mar (multiple antibiotic resistance) promoter of Escherichia coli in the presence of the activator MarA, SoxS, or Rob. *J Bacteriol* 179: 7410-7419.

Martin RG, Rosner JL (2004) Transcriptional and translational regulation of the marRAB multiple antibiotic resistance operon in Escherichia coli. *Mol Microbiol* 53: 183-191.

Martin RG, Bartlett ES, Rosner JL, Wall ME (2008) Activation of the Escherichia coli marA/soxS/rob regulon in response to transcriptional activator concentration. *J Mol Biol* 380: 278-284.

Miyashiro T, Goulian M (2007) Stimulus-dependent differential regulation in the Escherichia coli PhoQ-PhoP system. *Proc Natl Acad Sci USA* 104: 16305-16310.

Rodrigo G, Carrera J, and Jaramillo A (2011) Computational design of synthetic regulatory networks from a genetic library to characterize the designability of dynamical behaviors. *Nucleic Acids Res* 39: e138.

Salgado H, *et al.* (2013) RegulonDB (version 8.0): Omics data sets, evolutionary conservation, regulatory phrases, cross-validated gold standards and more. *Nucleic Acids Res* 41: D203-D13.

Salis HM, Mirsky EA, Voigt CA (2009) Automated design of synthetic ribosome binding sites to control protein expression. *Nat Biotechnol* 27: 946-950.

Schneiders T, Levy SB (2006) MarA-mediated transcriptional repression of the rob promoter. *J Biol Chem* 281: 10049-10055.

Seoane AS, Levy SB (1995) Characterization of MarR, the repressor of the multiple antibiotic resistance (mar) operon in Escherichia coli. *J Bacteriol* 177: 3414-3419.

Setty Y, Mayo AE, Surette MG, Alon U (2003) Detailed map of a cis-regulatory input function. *Proc Natl Acad Sci USA* 100: 7702-7707.

Swain PS, Elowitz MB, Siggia ED (2002) Intrinsic and extrinsic contributions to stochasticity in gene expression. *Proc Natl Acad Sci USA* 99: 12795-12800.

Rensing C, Grass G (2003) Escherichia coli mechanisms of copper homeostasis in a changing environment. *FEMS Microbiol Rev* 27: 197-213.

Vinué L, McMurry LM, Levy SB (2013) The 216-bp marB gene of the marRAB operon in Escherichia coli encodes a periplasmic protein which reduces the transcription rate of marA. *FEMS Microbiol Lett* 345: 49-55.

Viveiros M, Dupont M, Rodrigues L, Couto I, Davin-Regli A, Martins M, Pages JM, Amaral L (2007) Antibiotic stress, genetic response and altered permeability of E. coli. *PLoS ONE* 2: e365.

Wall ME, Markowitz DA, Rosner JL, Martin RG (2009) Model of transcriptional activation by MarA in Escherichia coli. *PLoS Comput Biol* 5: e1000614.

Weiss DS, Chen JC, Ghigo JM, Boyd D, Beckwith J (1999) Localization of FtsI (PBP3) to the septal ring requires its membrane anchor, the Z ring, FtsA, FtsQ, and FtsL. *J Bacteriol* 181: 508-520.